INTERNATIONAL JOURNAL FOR NUMERICAL METHODS IN ENGINEERING
Int. J. Numer. Meth. Engng 2006; **65**:2246–2264
Published online 14 November 2005 in Wiley InterScience (www.interscience.wiley.com). DOI: 10.1002/nme.1540

A hybrid regularization method for inverse heat conduction problems

Xianwu Ling[1,*,†], H. P. Cherukuri[2] and M. F. Horstemeyer[3]

[1]*Center for Advanced Vehicular Systems, Mississippi State University, Mail Stop 9618, 200 Research Blvd., Starkville, MS, U.S.A.*
[2]*Department of Mechanical Engineering and Engineering Science, University of North Carolina at Charlotte, U.S.A.*
[3]*Mechanical Engineering Department, Mississippi State University, MS, U.S.A.*

SUMMARY

This paper presents a hybrid regularization method for solving inverse heat conduction problems. The method uses future temperatures and past fluxes to reduce the sensitivity to temperature noise. A straightforward comparison technique is suggested to find the optimal number of the future temperatures. Also, an eigenvalue reduction technique is used to further improve the accuracy of the inverse solution. The method provides a physical insight into the inverse problems under study. The insight indicates that the inverse algorithm is a general purpose algorithm and applicable to various numerical methods (although our development was based on FEM), and that the inverse solutions can be obtained by directly extending Stolz's equation in the least-squares error (LSE) sense. Direct extension of the present method to the inverse internal heat generation problems is made. Four numerical examples are given to validate the method. The effects of the future temperatures, the past fluxes, the eigenvalue reduction, the varying number of future temperatures and local iterations for non-linear problems are studied. Copyright © 2005 John Wiley & Sons, Ltd.

KEY WORDS: heat conduction; inverse methods; regularization methods; eigenvalue reduction

1. INTRODUCTION

The success of the inverse heat conduction problems (IHCPs) lies largely in how the effect of noise in the measurements is regularized so that the solutions become least polluted. This is due to the fact that the inverse problem is inherently ill-posed. One consequence of the ill-posedness

*Correspondence to: Xianwu Ling, Center for Advanced Vehicular Systems, Mississippi State University, Mail Stop 9618, 200 Research Blvd., Starkville, MS 39759, U.S.A.
†E-mail: xling@cavs.msstate.edu

Contract/grant sponsor: Center for Advanced Vehicular Systems, Mississippi State University

is that a small noise in the measurements tends to produce a large error in the inverse solution. The sensitivity of the inverse solution to noise in the temperature measurements is caused by two *physical* constraints, namely, the temperature damping and the time delay of the interior response with respect to the surface changes [1]. Hence, the development of IHCP algorithms centres around the regularization techniques.

Various regularization methods have been put forward to reduce the sensitivity to the measurement errors. These methods include the digital filtering [2, 3], Tikhonov regularization [4], Alifanov iterative regularization [5], Beck's second (or the function specification) method [1, 6], the mollification method [7], the hyperbolic regularization [8], the eigenvalue reduction techniques [9–11], the conjugate gradient method [12] and the dynamic programming method [13], among many others. In our previous work [14, 15], a non-iterative, FEM-based sequential function specification method was developed. The present work is aimed at extending this method to include the Tikhonov regularization and the eigenvalue reduction techniques in addition to the future temperature regularization. First, in Tikhonov regularization method, additional functions in terms of the zero or higher order of the surface fluxes are added to the square error function method to reduce the fluctuation in the surface flux prediction. The additional terms are not physically required but numerically helpful. Second, we follow our previous development [15] in the sense that the future temperatures were employed to take into account the lagging and damping effects. One difficulty with Beck's second method exists in determining an optimal number of future temperatures. A number too small will still lead to oscillations or non-convergent solutions; while a number too large will oversmooth the surface fluxes. As such, an intermediate constant number is usually chosen based on trial and error. The combination of Beck's second method and Tikhonov method is called the trial function method [1]. The present hybrid method differs from the trial function method in three ways: first, it is non-iterative and uses the past heat fluxes in establishing the Tikhonov regularization; second, a local optimization technique, similar to the self-regularization method [4], was suggested for selecting the number of future temperatures; third, the eigenvalue reduction technique was also investigated together with the present hybrid method. The eigenvalue reduction was developed based on the characteristics of the IHCP, i.e. the high-frequency component of noise in the measurements will be amplified in the process of projecting to the surface, so the technique purposely discards the high-frequency modes when calculating the temperatures.

A brief outline of the paper is as follows: in Section 2, first, the inverse problem is described; next, the inverse algorithm is established; and lastly the eigenvalue reduction technique is presented. In Section 3, four numerical examples are provided to validate the method. Along with the validations, the effects of the future temperatures, of the past heat fluxes, and of the eigenmode are discussed, together with the optimal number of future temperatures and the local iteration for treating the non-linear problems.

2. MATHEMATICAL DESCRIPTION OF THE IHCP

In this section, we establish the inverse algorithm. First, we briefly describe the model problem following Ling *et al.* [14, 15]. Next, we apply the sequential function method to solve the model problem. And lastly, we introduce the eigenvalue reduction technique.

2.1. Model description

The definition of the inverse problem is briefly given as follows:

For a region subjected to the first and the second kind of boundary conditions (BCs), given the temperature measurements Y_m^i at $m = 1, 2, \ldots, M$ interior sites and $i = 1, 2, \ldots, \Im$ times, determine the unknown surface heat fluxes q_j^i at $j = 1, 2, \ldots, J$ at surface points for $i = 1, 2, \ldots, I$ computational time steps.

In setting up the above model problem, it is worth noting that (1) for the first kind of BCs on Γ_1, the surface temperatures are known; (2) for the second kind of BCs, the surface heat fluxes are partially known on Γ_2, and partially unknown on Γ_2'; (3) the unknown surface heat fluxes on Γ_2' are parameterized by J nodal variables. J is equal to or less than the node number on Γ_2'. In the latter case, interpolation of the heat fluxes on Γ_2' is assumed; (4) to ensure numerical stability, the computational time step-size is generally taken larger than the experimental one, so the total number of computations I is generally less than $\Im$.

2.2. Development of the inverse algorithm

The inverse algorithm below is developed following a methodology similar to that in References [14, 15]. First, the standard formulation based on the FEM for the direct heat conduction problem is given; second, the square error, with the addition of the past heat flux terms, is minimized; next, the physical interpretation is given for the normal equations, based on which the method is directly extended to the inverse heat generation problems; and then, a straightforward comparison technique is suggested for selecting the number of future temperatures; and lastly, a local iteration scheme is proposed for non-linear problems.

The explicit FEM for solving the direct heat conduction problem is given as

$$(\mathbf{M} + \Delta t\mathbf{K})\boldsymbol{\theta}^{i+1} = \mathbf{M}\boldsymbol{\theta}^{i} + \Delta t\mathbf{f}^{i+1} + \mathbf{c}^{i+1} \tag{1}$$

where $\mathbf{K}$ and $\mathbf{M}$ are the stiffness and the mass matrices, $\mathbf{f}^{i+1}$ is the heat flux force vector at $i+1$ time step, and $\mathbf{c}^{i+1}$ is a condensation vector obtained from the first kind of BCs. It is assumed the previous temperature $\boldsymbol{\theta}^i$ is known.

The problem now becomes finding the current heat fluxes $\mathbf{q}^{i+1}$ that best match the current and a few future temperature measurements. Meanwhile, to reduce any possible fluctuations in the flux prediction, it is enforced that the surface fluxes cannot change too dramatically between steps. Before we define the square error function, it is necessary to introduce the function specification method and distinguish the different time scales. The essence of the function specification method is to replace the unknown functions with a *chosen* form of functions (usually polynomials), so that the physical problem is changed into parameter estimations of the chosen functions. This may result in poor convergence, if the form of chosen functions are quite far away from the real case (which can be very complex), especially for the whole time-domain estimation, but does not pose a serious problem if solved sequentially. In the sequential function specification method, the surface heat fluxes are solved step by step, so that a simple form of the unknown function can be assumed to be a constant or a linear relation between two steps. More elaborate functions on time were found insignificant [16]. For simplicity, constant heat fluxes are assumed in our development. Figure 1 shows one example with a single unknown flux. Another point that needs to be clarified is the different time scales. An illustration of the various time scales is given in Figure 2, where ω represents the sampling rate, R represents the number of future temperatures, and P is the number of the past fluxes.

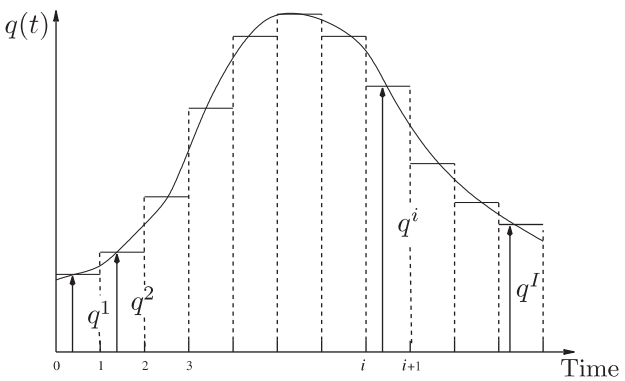

Figure 1. Function specification with constant fluxes.

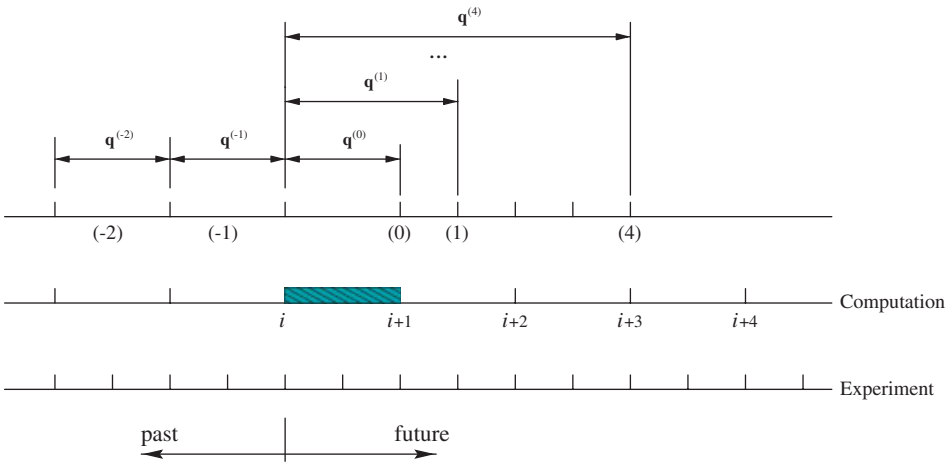

Figure 2. An illustration of different time scales. $\omega = 2$, $R = 4$, and $P = 2$.

Contrary to the direct heat conduction problem, a large computation time step is of necessity to ensure numerical stability of the inverse solutions. So, the computational time step Δt is generally larger than experimental one $\Delta\tau$, i.e.

$$\Delta t = \omega \Delta \tau$$

where the sampling rate ω is a positive integer. In addition, to provide maximum information to the inverse solution, the future temperatures are extracted at a time interval the same as $\Delta\tau$ [15]. When future temperatures are used, it is assumed that

$$\mathbf{q}^{i+1} = \mathbf{q}^{(0)} = \mathbf{q}^{(1)} = \cdots = \mathbf{q}^{(R)} \tag{2}$$

where the superscript (.) indicates that the index is measured with respect to the current time (not the initial one).

The inverse problem is solved in the least-squares error (LSE) sense. The square error norm, s^{i+1}, is given by

$$s^{i+1} = \sum_{m=1}^{M} \sum_{r=0}^{R} (Y_m^{(r)} - \tilde{\theta}_m^{(r)})^2 + \sum_{p=1}^{P} \sum_{j=1}^{J} w_j^{(-p)} (q_j^{(-p)} - q_j^{i+1})^2 \tag{3}$$

where $\tilde{\theta}_m^{(r)}$ is the calculated temperature at the measurement site, and $w_j^{(-p)}$ is a weight factor for the allowable heat flux jumps. Note, the past heat fluxes are added to the square errors in the same sense of the Tikhonov regularization. Unlike the trial function method, we enforce that the current heat fluxes are not allowed to change wildly with respect to the *past* fluxes. Zero-order regularization can be reduced by replacing $q_j^{(-p)}$ with zeroes in (3), yet the argument is that zero-order regularization can impose too strong a constraint if the real heat fluxes are far away from zeroes (which is often the case).

From Equation (1), the temperatures at (r) future time can be explicitly expressed as

$$\boldsymbol{\theta}^{(r)} = \mathbf{U}^{(r)} \mathbf{M} \boldsymbol{\theta}^i + \Delta t^{(r)} \mathbf{U}^{(r)} \mathbf{f}^{(r)} + \mathbf{d}^{(r)} \tag{4}$$

where $\mathbf{U}^{(r)} = [\mathbf{M} + \Delta t^{(r)} \mathbf{K}]^{-1}$, $\Delta t^{(r)} = t^{(r)} - t^n = \Delta t + r\Delta\tau$ and $\mathbf{d}^{(r)} = \mathbf{U}^{(r)} \mathbf{c}^{(r)}$. The calculated temperature $\tilde{\theta}_m^{(r)}$ at the mth measurement site is obtained by mapping the local index m (in $\tilde{\boldsymbol{\theta}}$) to its corresponding global node number m (in $\boldsymbol{\theta}$), i.e.

$$\tilde{\boldsymbol{\theta}}^{(r)} = \tilde{\mathbf{U}}^{(r)} \mathbf{M} \boldsymbol{\theta}^i + \Delta t^{(r)} \tilde{\mathbf{U}}^{(r)} \mathbf{f}^{(r)} + \tilde{\mathbf{d}}^{(r)} \tag{5}$$

where $\tilde{U}_{\mathsf{mn}}^{(r)} = U_{\mathsf{mn}}^{(r)}$, and where n ranges from 1 to N—the total number of nodes in the finite-element discretization.

The heat flux force at the (r)th future time, when utilizing Equation (2), can be written as

$$\mathbf{f}^{(r)} = \mathbf{D}\mathbf{q}^{(r)} = \mathbf{D}\mathbf{q}^{i+1} \tag{6}$$

where $\mathbf{D}$ is a constant matrix by the finite-element discretization.

Minimizing s^{i+1} with respect to q_j^{i+1} gives

$$\sum_{r=0}^{R} \sum_{m=1}^{M} X_{mj}^{(r)} (Y_m^{(r)} - \tilde{\theta}_m^{(r)}) + \sum_{p=1}^{P} \sum_{j=1}^{J} w_j^{(-p)} (q_j^{(-p)} - q_j^{i+1}) = 0 \tag{7}$$

where $X_{mj}^{(r)}$ is the sensitivity coefficient given by

$$X_{mj}^{(r)} = \frac{\partial \tilde{\theta}_m^{(r)}}{\partial q_j^{i+1}} \tag{8}$$

From (5) and (6), one obtains

$$X_{mj}^{(r)} = \Delta t^{(r)} \sum_{\mathsf{n}=1}^{\mathsf{N}} \tilde{U}_{\mathsf{mn}}^{(r)} D_{\mathsf{n}j} \tag{9}$$

Given (5), (9) and (7), now the governing equations read as

$$\sum_{r=0}^{R}\sum_{m=1}^{M}\sum_{j=1}^{J} X_{mj}^{(r)}X_{mj}^{(r)}q_j^{i+1} + \sum_{p=1}^{P}\sum_{j=1}^{J} w_j^{(-p)}q_j^{i+1}$$

$$= \sum_{r=0}^{R}\sum_{m=1}^{M} X_{mj}^{(r)}(Y_m^{(r)} - \tilde{\theta}_m^{(r)}) + \sum_{p=1}^{P}\sum_{j=1}^{J} w_j^{(-p)}q_j^{(-p)} \quad \text{for } j = 1, \ldots, J \tag{10}$$

or in the matrix form,

$$\left(\sum_{r=0}^{R}[\mathbf{X}^{(r)}]^{\mathrm{T}}\mathbf{X}^{(r)} + \sum_{p=1}^{P}\mathbf{w}^{(-p)}\right)\mathbf{q}^{i+1} = \sum_{r=0}^{R}[\mathbf{X}^{(r)}]^{\mathrm{T}}(\mathbf{Y}^{(r)} - \hat{\boldsymbol{\theta}}^{(r)}) + \sum_{p=1}^{P}\mathbf{w}^{(-p)}\mathbf{q}^{(-p)} \tag{11}$$

where $\hat{\boldsymbol{\theta}}^{(r)} = \tilde{\mathbf{U}}^{(r)}\mathbf{M}\boldsymbol{\theta}^{i} + \tilde{\mathbf{d}}^{(r)}$ is the *static* temperature for $\mathbf{q}^{i+1} = \mathbf{0}$. Note, 'static' here means that the temperature $\hat{\boldsymbol{\theta}}^{(r)}$ is only caused by the diffusion process for *zero* heat flux q^{i+1}.

When $\mathbf{w}^{(-p)} = \mathbf{0}$, the governing equations reduce to those in Reference [15], i.e.

$$\sum_{r=0}^{R}[\mathbf{X}^{(r)}]^{\mathrm{T}}\mathbf{X}^{(r)}\mathbf{q}^{i+1} = \sum_{r=0}^{R}[\mathbf{X}^{(r)}]^{\mathrm{T}}(\mathbf{Y}^{(r)} - \hat{\boldsymbol{\theta}}^{(r)}) \tag{12}$$

It is easily shown that this equation is a simple extension of Stolz's early work [17]. For multiple measurements, the Stolz's equation in the LSE sense can be written as

$$[\mathbf{X}^{(r)}]^{\mathrm{T}}\mathbf{X}^{(r)}\mathbf{q}^{(r)} = [\mathbf{X}^{(r)}]^{\mathrm{T}}(\mathbf{Y}^{(r)} - \hat{\boldsymbol{\theta}}^{(r)}) \tag{13}$$

We see that the right-hand side of Equation (13) gives the difference of the measured temperatures and the 'static' temperatures. Physically, this difference must be caused by any existing energy during the time period, whether the existing energy is from the external in the form of surface heat fluxes or from the internal in the form of heat generation. Hence, the left-hand side of Equation (13) links the energy source (here, in the form of the surface heat fluxes) to the difference of the temperatures—via the sensitivity coefficient in the LSE sense! When future temperatures are used, taking the summation of (13) over r, and using (6), one obtains exactly Equation (12). Note, that this deduction is based on the physical interpretation, no underlying numerical method (whether it is analytic, FDM, FEM, BEM, etc.) is involved. Thus, it can be seen that (11) is a general system of equations regardless of the underlying numerical methods (although our development here was based on the FEM), which also forms the first advantage of the present method over the previous method [15]. The independence of the underlying numerical methods is of special interest in calculating the sensitivity coefficient matrix. The current approach for calculating (9) involves inverting a square matrix of $\mathbf{M} + \Delta t^{(r)}\mathbf{K}$. For a small system with up to several hundreds of elements, this does not impose a problem, yet the computational time exponentially increases for a large system with thousands of elements (although to our best knowledge, no test problems have been reported for such a large system). Since the number of interior measurement points is often small, instead of inverting the whole matrix $\mathbf{M} + \Delta t^{(r)}\mathbf{K}$, the sensitivity coefficients are calculated only for the points at which the measurements are taken. In cases where the Green's function or the analytic solution are available, the computations of the sensitivity coefficient would be greatly speeded up.

The second advantage of the present method is that (12) permits much easier understanding of the method over its counterpart in Reference [15]. Basically, (12) is but an expression of cause and effect, with the right-hand side being the effect and the left-hand side being the cause. Based on the above argument, (12) can be interpreted as a direct solution method to Beck's second method (in which an iterative solution method is used). The third advantage of the present method is that, because of the physical interpretation, the governing equations should work for inverse problems of similar kind. One example is the inverse heat generation problems, in which case exactly the same development as above can be used. The resulting governing equations for the inverse heat generation problem are identical to (10) or (11), but $\mathbf{q}^{i+1}$ is interpreted as the source function of the internal heat generation, and $\hat{\boldsymbol{\theta}}^{(r)}$ is the 'static' temperature for *no* internal heat sources. The fourth advantage is that the past flux regularization is used, and as will be shown, greatly improves the initial accuracy of the calculations.

As mentioned above, one difficulty with Beck's second method lies in selecting the proper number of future temperatures. A number too small is not sufficient to suppress the error amplifications, while a number too large oversmooths the inverse results because of the assumption by Equation (2). Hence, R is usually chosen as a small constant based on trial and error. To our best knowledge, no systematic effort has been put forward to provide the optimal number of future temperatures. In our effort in devising R, first, it is allowed to vary (instead of being a constant) for different time steps. Second, it is based on the local variance of the temperature errors, which is defined as

$$s_m^{i+1} = \sqrt{\frac{1}{R+1}\sum_{r=0}^{R}(Y_m^{(r)} - \tilde{\theta}_m^{(r)})^2} \quad \text{for } m = 1, 2, \ldots, M$$

where s_m^{i+1} is a function of R. Assume that the measurements from one site do not interface with those from the other, the argument is that for whatever R chosen, the minimum of s_m^{i+1} goes to not zero but the global variance of the temperature measurement σ_m (because of the *inherent* nature of the noise). Assume that $\tilde{\theta}_m^{(r)}$ be calculated accurately (thus $\mathbf{q}^{i+1}$ being exact), then $(s_m^{i+1})^2$ follows the χ^2 distribution since the errors in the temperature measurement are generally assumed to follow the Gaussian distribution. Hence, for large R's, $|s_m^{i+1} - \sigma_m|$ approaches zero. For very small R's, $|s_m^{i+1} - \sigma_m|$ is uncertain but remains bounded (cf., Reference [18]). Similar arguments have been used by Tikhonov [4] in developing the self-regularization method. In Reference [1], the mean of the errors is also assumed to be zero. So, we define

$$\varepsilon(R) = \frac{1}{M}\sum_{m=1}^{M}\left[|s_m^{i+1} - \sigma_m| + \frac{1}{R+1}\left|\sum_{r=0}^{R}(Y_m^{(r)} - \tilde{\theta}_m^{(r)})\right|\right] \tag{14}$$

to represent the local error level for different R's. (Note, the last term in the right-hand side of (14) defines the absolute mean error.) In our implementation, for each computational time step, $R_{\min}$ and $R_{\max}$ are also given. $R_{\min}$ is to ensure the stability of the inverse solutions, $R_{\max}$ is a big number. The actual R used corresponds to the one which gives the minimum ε. It is worth mentioning the importance of data redundancy of the temperature measurements. Since we use the same time step for the future temperatures as the experimental one, it is suggested the experiment time interval be made small (thus, more experiment data are available) so that $R_{\max}$ can be set large enough to ensure the square errors follow the χ^2 distribution. Also worth mentioning is that the input temperature errors (whether from physical or numerical

experiments) should not overwhelm the temperature changes caused by the targeted heat fluxes, otherwise, large oscillations are inevitable.

Finally, for highly non-linear problems, a local iteration scheme is given as follows. First, we note that by quasi-linearization [1], the previous temperatures $\boldsymbol{\theta}^i$ are used to evaluate $\mathbf{M}$ and $\mathbf{K}$. So, in this local iteration, when the current heat fluxes are solved, the current temperatures are updated, $\mathbf{M}$ and $\mathbf{K}$ are re-evaluated and the current heat fluxes are recalculated, and so with the current temperatures, and so on. The iteration stops when the relative temperature error for the lth local iteration, defined as

$$\varepsilon^l = \|\boldsymbol{\theta}^{i,l+1} - \boldsymbol{\theta}^{i,l}\| / \|\boldsymbol{\theta}^{i,l}\|$$

is very small (set to 0.001 in our calculations).

2.3. Eigenvalue reduction technique

As stated earlier, the eigenvalue reduction was intended to filter out the high-frequency modes. When the current heat fluxes are solved, instead of using (4) to solve the current temperatures, the eigensystems are evoked. Also, the eigensystems are used to calculate the 'static' temperatures $\hat{\boldsymbol{\theta}}^{(r)}$.

The eigensystems are solved based on $\mathbf{M}\dot{\boldsymbol{\theta}} + \mathbf{K}\boldsymbol{\theta} = \mathbf{0}$. The heat conduction equations in the eigensystems can be written as

$$\bar{\mathbf{M}}\dot{\mathbf{T}} + \bar{\mathbf{K}}\mathbf{T} - \bar{\mathbf{f}} = 0 \tag{15}$$

where

$$\bar{\mathbf{M}} = \boldsymbol{\Phi}^{\mathrm{T}}\mathbf{M}\boldsymbol{\Phi}, \quad \bar{\mathbf{K}} = \boldsymbol{\Phi}^{\mathrm{T}}\mathbf{K}\boldsymbol{\Phi} \quad \text{and} \quad \bar{\mathbf{f}} = \boldsymbol{\Phi}^{\mathrm{T}}\mathbf{f}$$

and where $\boldsymbol{\Phi} = [\boldsymbol{\phi}_1, \boldsymbol{\phi}_2, \ldots, \boldsymbol{\phi}_N]$ is the $N \times N$ matrix of eigenvectors. $\mathbf{T} = \boldsymbol{\Phi}^{\mathrm{T}}\boldsymbol{\theta}$ is the temperature vector in the modal domain. Note, (15) forms N independent equations because of the orthogonality conditions, i.e.

$$\boldsymbol{\phi}_i^{\mathrm{T}}\mathbf{M}\boldsymbol{\phi}_j = 0, \quad \boldsymbol{\phi}_i^{\mathrm{T}}\mathbf{K}\boldsymbol{\phi}_j = 0 \quad \text{for } i \neq j$$

The first $\mathfrak{N}$ ($\leqslant \mathrm{N}$) lowest eigenvalues are selected from the full mode. Hence, the dimension of $\boldsymbol{\Phi}$ reduces to $N \times \mathfrak{N}$. Finally, the temperatures are recovered from the reduction mode by $\boldsymbol{\theta} = \boldsymbol{\Phi}^{\mathrm{T}}_{N\times\mathfrak{N}}\mathbf{T}$.

Note that the eigenvalue reduction technique is suitable for the linear problems. For the non-linear case, because of the quasi-linearization process, it can still be applied for each computational time step. However, as shown from our numerical examples, the improvement of the solution accuracy by the technique is insignificant, but the computational time increases much more in solving the eigensystems.

3. NUMERICAL EXAMPLES

In this section, four numerical examples are provided to validate the above method. These include a one-dimensional (1D) plate subjected to a triangular-shape heat flux, a 1D plate with a square internal heat source in the mid-plane, a two-dimensional (2D) plate subjected to two

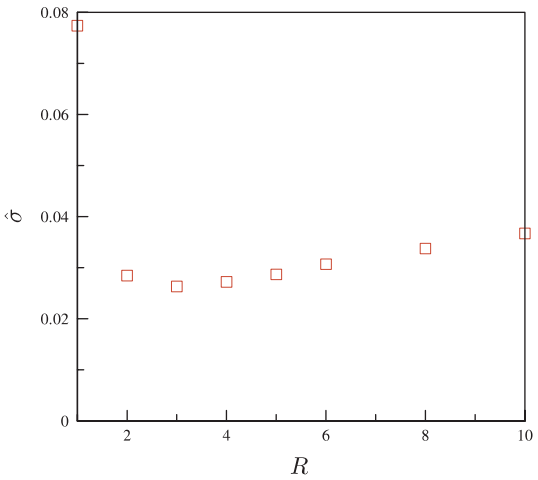

Figure 3. The variance of $\hat{\sigma}$ with R. $N = 37$.

trapezoid-like fluxes, and lastly a highly non-linear problem of a 2D axisymmetric cylindrical wall with 3 zig-zag shape fluxes. All the example problems are taken from the published literature.

3.1. Case 1: triangular surface heat flux at $x = 0$

This example is taken from Beck [1], and has been considered by many authors (cf., Reference [15]). A flat plate is subjected to a triangular heat flux at $x = 0$ and insulated at $x = L$. The experimental temperatures were simulated from the analytical solution at $x = L$ at a time interval of 0.02. Noise was simulated by data truncating [1] or by adding a random component to the exact temperature as follows:

$$\tilde{Y}_m^l = Y_m^l + \sigma \varepsilon_m^l$$

where ε_m^l is the standard Gaussian distribution given by [19]

$$\varepsilon_m^l = \sum_{l=1}^{12} RN_l - 6.0 \tag{16}$$

Here, RN_l is a random number uniformly distributed between 0 and 1.

Let the mean square error of the estimated heat flux be defined as

$$\hat{\sigma} = \left[\frac{1}{I} \sum_{i=1}^{I} (q_i - q_i|_{\text{exact}})^2 \right]^{1/2}$$

Figure 3 plots the variation of $\hat{\sigma}$ versus R (which is taken as a constant in each calculation). The accuracy of the results depends on the number of future temperatures. As expected, too small or too large a constant R both degrade the accuracy. Overall, the present results agree excellently with the exact solution. To show the effect of varying R, Figure 4 shows a comparison of

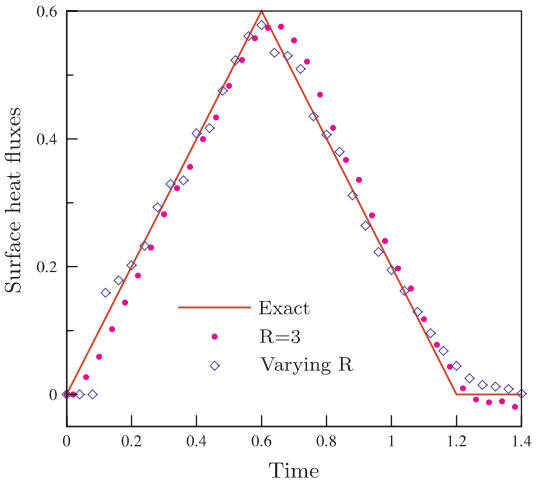

Figure 4. A comparison of calculated heat fluxes for constant and varying R. $N = 37$.

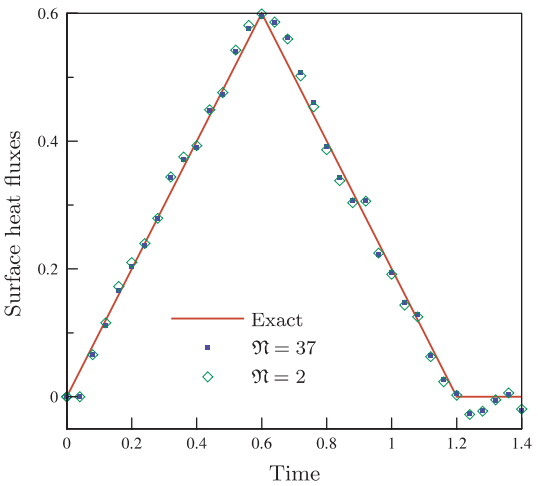

Figure 5. A comparison of calculated heat fluxes for different number of eigenmodes ($\mathfrak{N}$) for $R = 2$.

the calculated heat fluxes for a constant $R = 3$ (with $\hat{\sigma} = 2.63 \times 10^{-2}$, which gives the best accuracy for the constant R calculations) and the varying R (with $\hat{\sigma} = 2.32 \times 10^{-2}$). Obviously, varying R improves the accuracy of the results.

Next, the effect of the eigenvalue reduction is shown in Figure 5. It is seen that the two lowest eigenmodes can give nearly the same accuracy as when all the modes for the discrete problem ($\mathfrak{N} = \mathrm{N} = 37$) are considered. A simple explanation is given as follows. The inner

product of $\boldsymbol{\theta}$ with itself gives

$$(\boldsymbol{\theta}, \boldsymbol{\theta}) = \sum_{i=1}^{\mathfrak{N}} T_i^2$$

From (15), it can be shown that

$$T_i = \left(1 - \frac{\bar{f}_i}{\lambda_i}\right) \mathrm{e}^{-\lambda_i t}$$

where λ_i is the ith eigenvalue given by $\bar{M}_{ii}/\bar{K}_{ii}$. Defining

$$\zeta(\mathfrak{N}) = \sum_{i=1}^{\mathfrak{N}} T_i^2/(\boldsymbol{\theta}, \boldsymbol{\theta}) \tag{17}$$

our calculations show that $\zeta = 0.99$, 1.00 for $\mathfrak{N} = 1, 2$, and remains at 1.00 for $\mathfrak{N} = 3, 4, \ldots, 37$. Thus, $\mathfrak{N} = 2$ is sufficient to keep the accuracy of the solutions.

The effect of the past heat flux regularization is considered next. The input data for this case was taken directly from Table 5.3 from Beck [1] with a normalized $\sigma = 0.0017$. The weight is applied equally to all the surface fluxes, but decays exponentially with time in the following form:

$$w_j^{(-p)} = w_t \mathrm{e}^{-p\Delta t} \quad \text{for } p = 1, 2, \ldots, P$$

where w_t is a common weight factor. For the case under study, we chose $P = 2$, $w_t = 10^{-8}$ for $t \leqslant 0$ and $w_t = 10^{-9}$ for $t > 0$. Such a choice is made to reduce any initial large oscillations (cf., Reference [14]). The surface heat fluxes are shown in Figure 6. Also shown in the figure is Beck's result for $R = 2$. The past heat flux regularization significantly improves the results for the early times. In comparison with Beck's result, we have $\hat{\sigma}|_{P=0} = 2.68 \times 10^{-2}$,

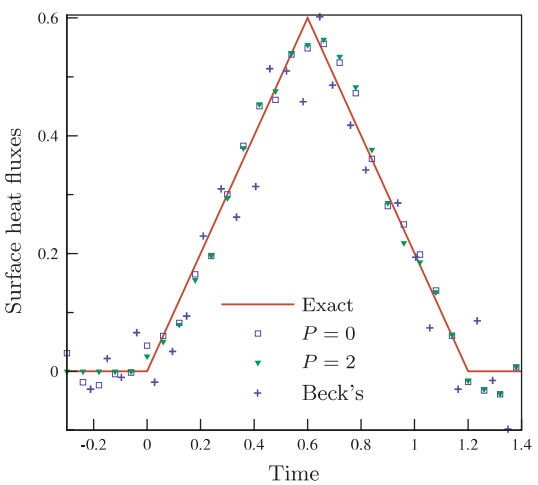

Figure 6. A comparison of calculated heat fluxes for different P. $R = 2$.

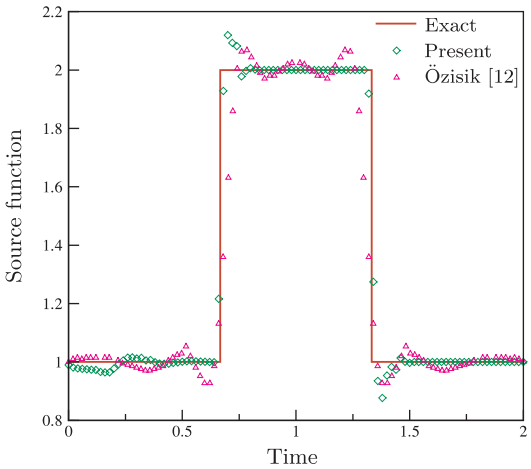

Figure 7. A comparison of the heat source function.

$\hat{\sigma}|_{P=2} = 2.60 \times 10^{-2}$, and $\hat{\sigma}|_{\text{Beck's}(R=2)} = 5.60 \times 10^{-2}$. Because of the large w_t for $t \leqslant 0$, the initial oscillation as seen in the case of $P = 0$ is suppressed when $P = 2$. Like the future temperature, the past heat fluxes may oversmooth the results if P or w_t is too large.

3.2. Case 2: 1D internal heat generation

To validate the optimization scheme for R, a linear heat conduction in a plate of unitary dimensionless thickness is considered following Özisik [12]. The plate is initially at zero temperature and insulated at both ends. A plane heat source $g_p(t)$ is placed at $x = 0.5$. The heat source is taken to be of the form: $g_p(t) = 1$ for $0 \leqslant t < \frac{2}{3}$ and $t > \frac{4}{3}$, and $g_p(t) = 2$ for $\frac{2}{3} \leqslant t \leqslant \frac{4}{3}$. The temperatures at $x = 1$ are generated by the analytical solution and used as the input for the inverse problem.

In Figure 7, the heat source predicted by the present method is compared with that of Özisik [12] using the conjugate gradient method with the adjoint problem. The varying R with time is shown in Figure 8 with $R_{\min} = 0$ and $R_{\max} = 25$. The exact $g_p(t)$ is shown at the bottom of Figure 8. The present results agree well with most part of the exact solution, except near the discontinuities, where, similar to the conjugate gradient method, some oscillations are observed. In terms of accuracy, $\hat{\sigma}|_{\text{current}} = 0.044$, and $\hat{\sigma}|_{\text{Özisik}} = 0.085$. One interesting feature of the present method is about the changes of R. Close to the discontinuities of $g_p(t)$, the optimal scheme senses the sudden change in the temperatures. Consequently, R suddenly drops (indicated by the arrows in Figure 8), so that $g_p(t)$ is allowed to make rapid changes also. As expected, it appears the first time that varying R has been employed.

3.3. Case 3: 2D planar heat conduction

Our next example is taken from Tandy [9]. A 2D slab, as discretized in Figure 9, is subjected two trapezoid-like fluxes. Temperature measurements are taken at nodes 11 and 23. For comparison purposes, the noise level $\sigma = 4$. Past flux regularization is used with $w_t = 0.1$. The

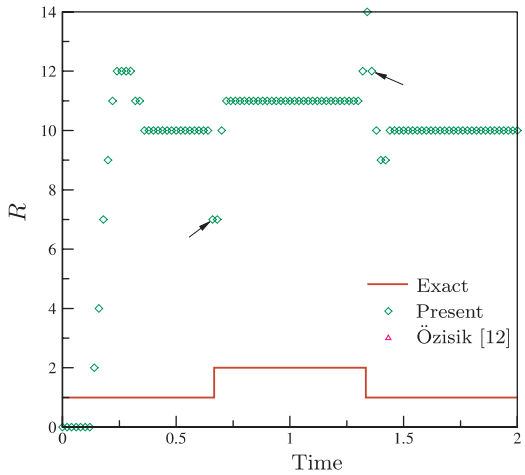

Figure 8. The varying R versus time.

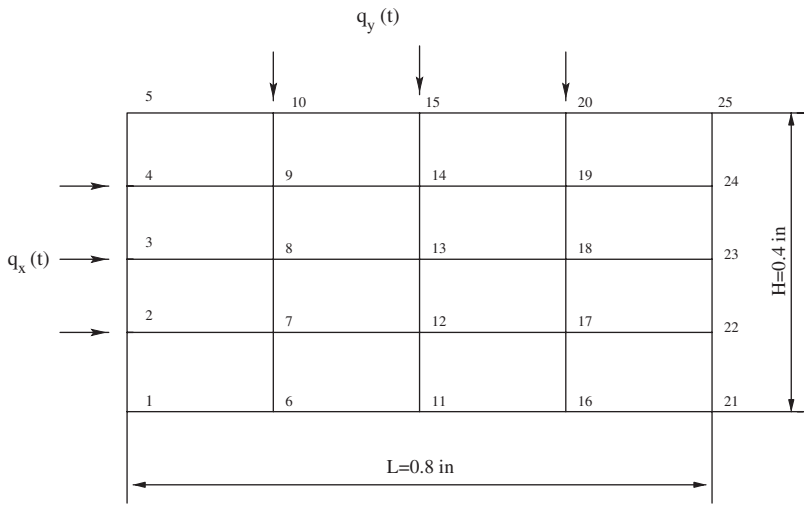

Figure 9. FEA model of the 2D slab with two unknown fluxes.

predicted heat fluxes are shown in Figures 10 and 11 using the full eigenmodes with $R_{\min} = 2$ and $R_{\max} = 10$. Also shown in the figures are the results given by the dynamic programming technique [9]. The present results are less oscillatory and closer to the real solutions. This is also true with the reduced eigenmode $\mathfrak{N} = 6$ (not shown here). But, the reduced eigenmode $\mathfrak{N} = 6$ is less accurate than the full eigenmode. The same thing can be observed from Reference [9]. Hence, the eigenvalue reduction does not necessarily guarantee more accuracy of the inverse solution. It is noted that ε_m^l as generated by (16) changes signs almost for

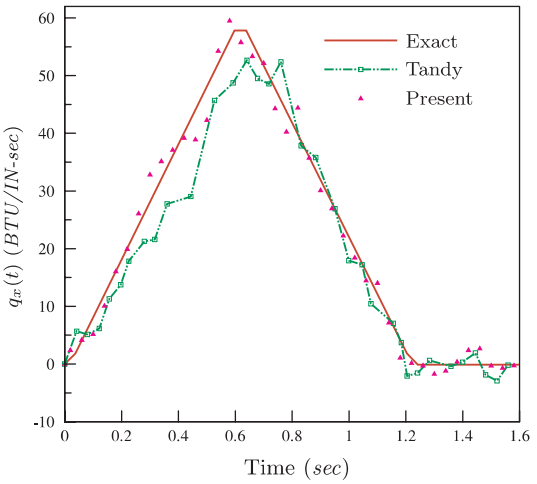

Figure 10. Heat flux $q_x(t)$ using 25 modes and varying R.

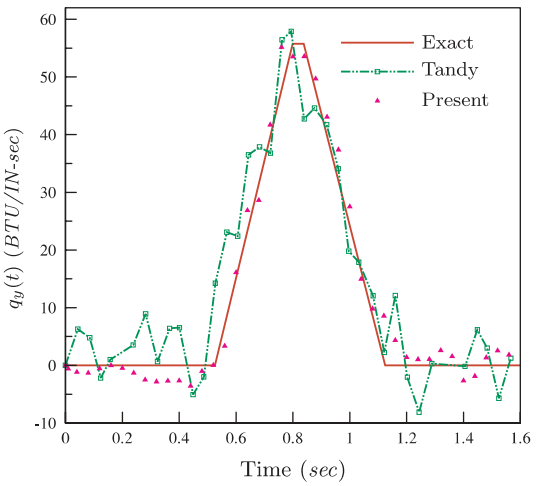

Figure 11. Heat flux $q_y(t)$ using 25 modes and varying R.

every i. This caused some special difficulties for the initial time when the errors are larger than the temperature changes. As in Cases 1 and 2, the past flux regularization significantly improves the initial behaviour. Figure 12 shows the variation of R with time. The pattern of the varying R here is more subtle to analyse. It is affected to a large degree by the uncertainty of the temperature errors. Roughly, it can been seen that each time $q_y(t)$ takes a turn (at $t = 0.52, 1.12$), R changes.

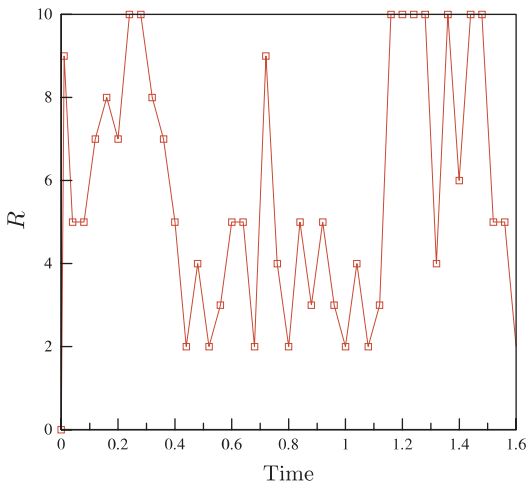

Figure 12. The variation of R versus time for 2D planar problem. $\sigma = 4$, $R_{\min} = 2$ and $R_{\max} = 10$.

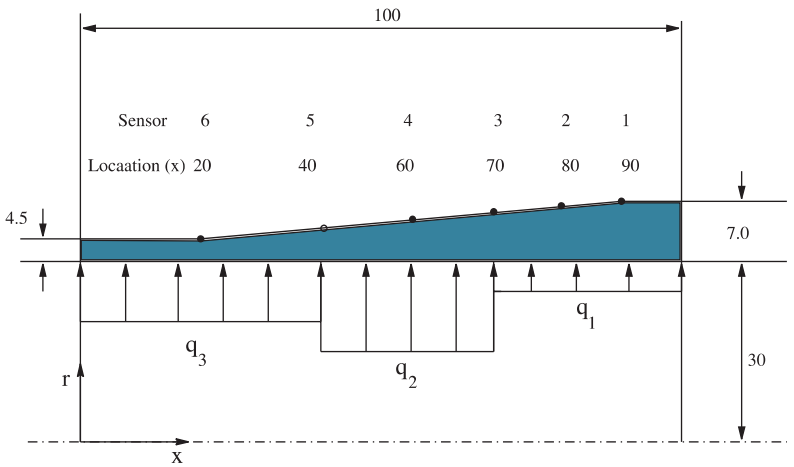

Figure 13. Geometry and sensor location for simulated experiment. All dimensions in mm.

3.4. Case 4: 2D axisymmetric highly non-linear problem

Our last example validates the proposed method against a highly non-linear problem. The model is illustrated in Figure 13. It is based on the test case given in Reference [20] and intended to simulate the axisymmetric cylinder wall of an internal combustion engine. Due to lack of data, direct comparison with Reference [20] is not available.

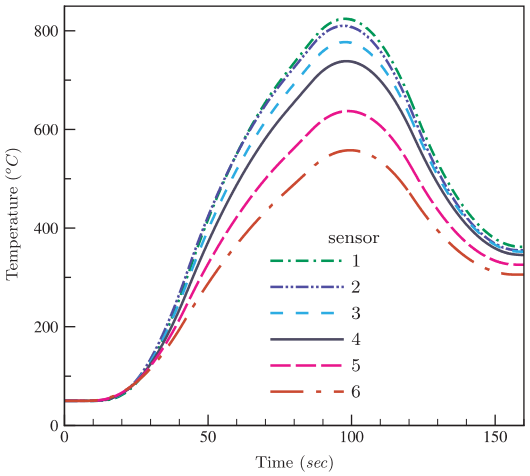

Figure 14. Simulated temperatures for $\sigma = 0$.

The thermal conductivity is assumed to be temperature dependent and given by

$$k(\theta) = k_0 + (k_1 - k_0)\,\frac{\theta - \theta_0}{\theta_1 - \theta_0}$$

where $k_0 = k(\theta = 0\,^\circ\mathrm{C}) = 2(\mathrm{W/m} - \mathrm{C})$ and $k_1 = k(\theta_1 = 1000\,^\circ\mathrm{C}) = 22(\mathrm{W/m} - \mathrm{C})$. The volume heat capacity is taken as a constant $3.8 \times 10^6\,\mathrm{J/m^3\,C}$. Figure 14 shows the 'experimental' data for the six sensors. The thermal conductivity changes nearly one order of magnitude under the thermal loading conditions.

We consider only the cases using the 'exact' data as the input. Figure 15 shows the predicted heat fluxes when no local iterations are used, and Figure 16 shows the predicted heat fluxes when the local iterations are evoked. Small oscillations can be seen for the case when no local iterations are used. The oscillations disappear when R is increased to three (not shown here). Interestingly, the oscillations also disappear when local iterations are used. Generally, the local iterations tend to improve the overall accuracy of the inverse solutions. However, for large R, the local iterations may decrease the accuracy; therefore, a real solution is closer to the average of the solutions with and without the local iteration. It is also found that usually two to three such local iterations would satisfy the stopping criterion. In places where the temperatures change rapidly, more iterations are observed as expected.

4. CONCLUSION

In conclusion, the present work proposes a hybrid regularization method for the inverse heat conduction problems. The method includes the features of the sequential function specification method, the Tikhonov method, the eigenvalue reduction method, and the self-regularization method. A physical interpretation is given for the governing equation, which enables a direct

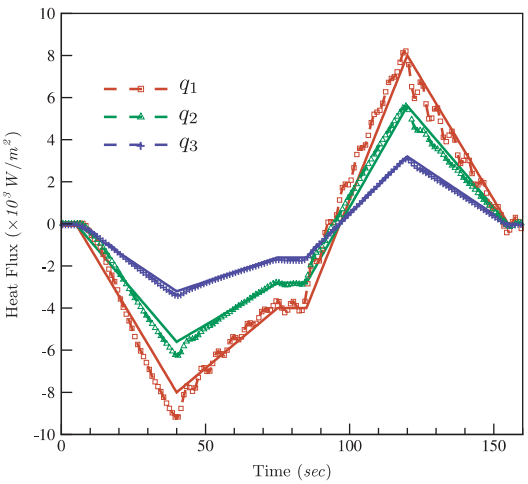

Figure 15. Estimated heat flux for $\sigma = 0$ and $R = 2$ with no local iteration.

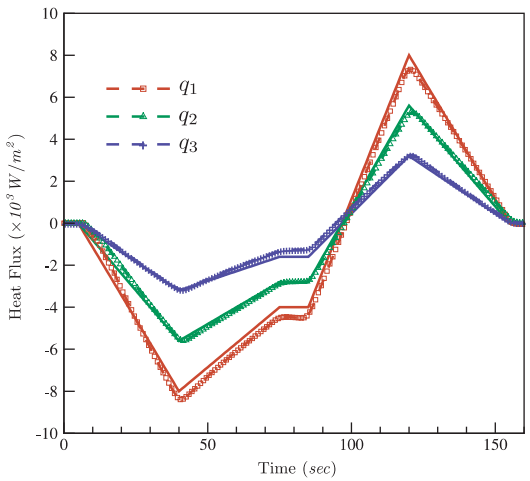

Figure 16. Estimated heat flux for $\sigma = 0$ and $R = 2$ with local iterations.

extension of the method to the inverse heat generation problems and removes the dependence of the method on the underlying numerical method.

The future temperatures are found to be the most important factors in determining the surface fluxes. Too small a number of future temperatures produces an oscillatory (or non-convergent) result and a number too large may oversmooth the results. An optimal number of future temperatures is suggested based on the idea of the self-regularization. In the case where there exist sharp changes in the surface heat fluxes, the optimal scheme predicts a change of R. Although the optimal scheme is tested against the numerical cases under study, we do not claim

the scheme to be a golden rule, especially regarding the choice of $\varepsilon(R)$. The reason is twofold. First, the uncertainty of the measurement errors to a large degree affects the local behaviour of $\varepsilon(R)$. Second, the distribution characteristics may not hold true for a small number of sampling future temperatures. But at least the present effort appears to be a worthwhile attempt in optimizing R. Further investigation is needed in understanding this aspect.

The past heat fluxes can improve the accuracy of the inverse solutions. However, like the future temperatures, they may smear out sharp changes in the heat fluxes if overweighed. One situation in which the past heat flux regularization is suggested is at the beginning of the calculations when the level of the heat flux before the start of the heating/cooling process is known *a prior* (usually zeroes). For all the cases under study, it removes the initial oscillation (if it exists) in the predictions.

As for the eigenvalue reductions, we show that in one aspect, a very small number of eigenvalues of a large system can be used to produce a very close result to the full-mode solution; on the other aspect, as the system is discretized into more elements, the eigenvalues tends to be more uniformly distributed, hence, more eigensystems should be used according to (17). Yet, the computation cost increases exponentially with increasing N. This is especially true for the non-linear problem for which the eigensystems have to be solved for each computational step. The overall effect of eigenvalue reduction is found to be limited.

The local iteration scheme in general tends to improve the accuracy of the inverse solutions and may suppress artificial oscillations that may be present. Either large R or the local iterations can reduce the solution oscillations, but when used simultaneously, the results worsen. So, a balance between a large R and using local iterations is suggested.

REFERENCES

1. Beck JV, Blakwell B, St. Clair CR. *Inverse Heat Condition*: *Ill-posed Problems*. Wiley: New York, 1985.
2. Hills RG, Hensel EC. One-dimensional nonlinear inverse heat conduction technique. *Numerical Heat Transfer* 1986; **10**:369–393.
3. Hensel EC, Hills RG. An initial value approach to the inverse heat conduction problem. *Transactions of the AMSE*, *Journal of Heat Transfer* 1986; **108**:248–256.
4. Tikhonov AN, Arsenin VY. *Solution of Ill-posed Problems*. V.H. Winston and Sons: Washington, DC, 1977.
5. Alifannov OM. *Inverse Heat Transfer Problems*. Springer: New York, 1994.
6. Bass BR. Application of the finite element method to the nonlinear inverse heat conduction problem using Beck's second method. *Transactions of the ASME* 1980; **102**:168–176.
7. Murio DA. *The Mollification Method and the Numerical Solution of Ill-posed Problems*. Wiley: New York, 1993.
8. Weber CF. Analysis of the ill-posed inverse heat conduction problem. *International Journal of Heat and Mass Transfer* 1981; **24**(11):1783–1792.
9. Tandy DF, Trujillo DM, Busby HR. Solution of inverse heat conduction problems using an eigenvalue reduction technique. *Numerical Heat Transfer* 1986; **10**:597–617.
10. Park HM, Lee JH. Solution of an inverse heat transfer problems by means of empirical reduction of modes. *Zeitschrift fur Angewandte Mathematik und Physik* 2000; **51**:17–38.
11. Videcoq E, Petit D. Model reduction for the resolution of multidimensional inverse heat conduction problems. *International Journal of Heat and Mass Transfer* 2001; **44**:1899–1911.
12. Özisik MN, Orlande HRB. *Inverse Heat Transfer*. Taylor-Francis: New York, 2000.
13. Trujillo DM, Busby HR. *Practical Inverse Analysis in Engineering*. CRC Press: New York, 1997.
14. Ling X, Keanini RG, Cherukuri HP. A non-iterative finite element method for inverse heat conduction problems. *International Journal for Numerical Methods in Engineering* 2003; **56**:1315–1334.
15. Ling X, Keanini RG, Cherukuri HP. An implicitly regularized, non-iterative finite element method for inverse heat conduction problems. *Computational Mechanics* 2005, in press.

16. Beck JV *et al*. Comparison of some inverse heat conduction methods using experimental data. *International Journal of Heat and Mass Transfer* 1996; **39**(17):3649–3657.
17. Stolz Jr G. Numerical solutions to an inverse problem of heat conduction for simple shapes. *Journal of Heat Transfer* (ASME) 1960; **82**:20–26.
18. Graham NY. Smoothing with periodic cubic splines. *Bell System Technical Journal* 1983; **62**:101–110.
19. Hovanessian SA, Pipes LA. *Digital Computer Methods in Engineering*. McGraw-Hill: New York, 1969.
20. Osman AM, Dowding KJ, Beck JV. Numerical solution of the general two-dimensional inverse heat conduction problem. *Transactions of the ASME* 1997; **119**:38–45.

